

Scaling properties of pyrex and silicon surfaces blasted with sharp particles

Z. Moktadir* and M. Kraft

*School of Electronics and Computer Science, Southampton University, Southampton, SO17 1BJ, United Kingdom**

H. Wensink

Transducers Science and Technology MESA+ Research Institute University of Twente, The Netherlands

The blasting of brittle materials with sharp particles is an important fabrication technology in many industrial processes. In particular, for micro-systems, it allows the production of devices with feature sizes down to few tens of microns. An important parameter of this process is the surface roughness of post-blasted surfaces. In this work the scaling properties of Pyrex glass and silicon surfaces after bombardment with alumina particles is investigated. The targets were bombarded at normal incidence using alumina particles with two different average sizes, $29\mu m$ and $9\mu m$, respectively. This investigation indicates that the resulting surfaces have multifractal properties. Applying multifractal detrended fluctuation analysis (MFDFA) allowed us to determine the singularity spectrum of the surfaces. This spectrum did not depend on the target material or on the size of the particles. Several parameters quantifying relevant quantities were determined. We argue that for scales below $5\mu m$, fracture processes are dominant while at large scales long range correlations are responsible for the multifractal behaviour.

PACS numbers:

I. INTRODUCTION

Powder blasting technology is among several techniques used in the micro-machining [1, 2, 3] of devices on silicon and other materials. With such abrasive techniques, one can achieve high erosion rates; higher than those that can be obtained with conventional dry, or wet etching processes; such as plasma etching or chemical etching. In the field of micro-electromechanical-systems (MEMS), powder blasting has already been used for the fabrication of inertial sensors[2], peristaltic micro-pumps[3] and miniaturized capillary electrophoresis chips[4]. Erosion with sharp particles is also a widely used technique in aerospace and automotive industries. Because of its involvement in many applications, it is important to investigate the surface morphology of blasted surfaces resulting from erosion since the performance of many devices will depend on the surface roughness. Such investigation will also give an insight into the physical mechanisms at work during the bombardment of materials with particles. The mechanisms involved in the erosion of brittle materials with sharp particles have been the subject of several studies. Several models have been developed [5, 6] that are based on simple static indentation theory. These models empirically relate the erosion rate to the material's properties such as the fracture toughness, the hardness and the Young modulus of the material. These models simply state that an indentation force is generated by the impact of bombarding particles which, in turn, results in the formation of crack patterns. Some cracks penetrate the material radially away from the surface into the bulk material; oth-

ers will nucleate and form a lateral ring parallel to the surface[7, 8, 9]. The radial cracking process was extensively studied [10, 11] and was used as a method for materials toughness measurement[12]. Lateral cracks are responsible for the removal of material in abrasive and wear experiments on brittle materials[13, 14, 15].

In separate studies, substantial work was dedicated to the understanding of fracture surfaces [16] in brittle materials. These studies focus on the scaling properties of fracture surfaces resulting from an applied load on the material. These surfaces are found to be self-affine, i.e. the root-mean-square surface fluctuations, averaged over a distance L follows the scaling relation[17]:

$$r \sim L^\alpha \quad (1)$$

where the scaling exponent α is often called the roughness or the Hurst exponent. In a variety of materials, the value of α was found to be approximately 0.8 over two or three decades of scaling range. For this reason, it was conjectured to be universal i.e. independent of the material (ductile or brittle), the fracture mode and the fracture toughness [16, 18, 19]. However, this universality was questioned since the discovery of a second exponent at the nanometer scale[20, 21, 22]. The value of this second exponent is significantly smaller than 0.8 and close to 0.5. To explain this fact, it was proposed that the fracture front could be imagined as a line moving through a random medium. Thus, the evolution of the crack front can be described by a local nonlinear Langevin equation [23, 24, 25] which predicts a crossover between two regimes corresponding to $\alpha = 0.5$ at small scales and to $\alpha = 0.75$ at large scale. In the framework of this model, the crossover length decreases rapidly with the crack speed which was also predicted by numerical simulations[26].

The present work is dedicated to the study of the scal-

*Electronic address: zm@ecs.soton.ac.uk

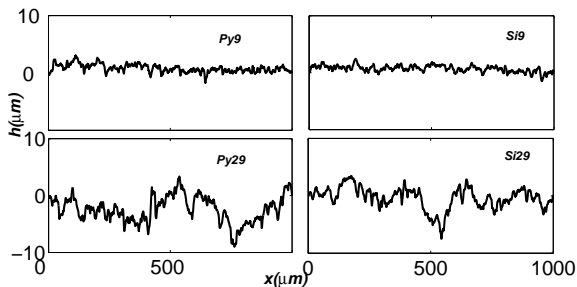


FIG. 1: Surface profiles after blasting of Pyrex and silicon with particles of size $\delta = 9\mu m$ (Py9 and Si9), and with particles of size $\delta = 29\mu m$ (Py29 and Si29).

ing properties of surfaces resulting from a bombardment by sharp particles. Pyrex glass (borosilicate glass) and silicon were the materials used in this investigation. We will investigate the effect of the material and the size of the bombarding particles on those properties.

II. EXPERIMENTS

In the experiments carried out, surfaces are exposed to a directed particle jet, which results in mechanical material removal. The particles are accelerated towards the target with a high-pressure air flow through a circular nozzle (with a diameter of $1.5\mu m$). The particles hit the target under normal incidence, with an average speed of 290 m/s, in a ventilated box. A lateral movement of the target ensures an evenly etched surface. The average diameter of the bombarding alumina particles was $9\mu m$ and $29\mu m$, respectively. We performed measurements on one-dimensional cuts of blasted surface using a mechanical surface profiler (Sloan Dektak II), over a length of 1 mm. Each scanned profile is made of 8000 data points. Typical profiles obtained after blasting Pyrex and silicon surfaces by alumina particles are shown in figure 1. Note the difference in the roughness amplitude in the two cases corresponding to different particle sizes. Large amplitudes are obtained when the targets are blasted by large particles. The typical rms surface roughness is $\sigma = 0.7\mu m$ and $\sigma = 0.65\mu m$ for Pyrex and silicon respectively, when $9\mu m$ particles are used. In table I, measured values of the surface rms roughness are shown, as a function of the bombarding particle sizes and the target material. Samples bombarded with particles having a diameter δ are denoted $X\delta$, where X denotes the material's symbol. For example *Si29* means silicon bombarded with particles having a diameter of $29\mu m$.

Particles size	$9\mu m$	$29\mu m$
Pyrex	$0.7 \pm 0.02\ \mu m$	$2.2 \pm 0.02\ \mu m$
Silicon	$0.65 \pm 0.01\ \mu m$	$2.3 \pm 0.01\ \mu m$

TABLE I: Values of the rms roughness as a function of the particles size and the target material.

Sample	α_1	α_2	$\xi(\mu m)$
Si9	0.77 ± 0.02	0.4 ± 0.01	4.8
Si29	0.81 ± 0.01	0.55 ± 0.002	4.7
Py9	0.74 ± 0.02	0.32 ± 0.003	4.7
Py29	0.8 ± 0.02	0.53 ± 0.04	5.2

TABLE II: Values of the roughness exponents and the crossover length ξ for the four samples.

III. SCALING PROPERTIES OF BLASTED SURFACES

A. Global scaling exponents

We first investigate the global scaling behaviour of the blasted surfaces by calculating the height-height correlation function defined as :

$$C(r) = \left\langle (h(x+r) - h(x))^2 \right\rangle^{1/2} \quad (2)$$

where the outer brackets mean the average over all positions x and $h(x)$ defines the surface profile. This function measures how correlated two points are on the profiles at a distance r of each other. If the surface is self-affine then $C(r) \propto r^\alpha$, over the scaling range. Here, α is the roughness exponent to be determined. We computed $C(r)$ for one dimensional cuts and averaged the result over a total of ten scanned profiles. In figure 2 we plot $C(r)$ for $2\mu m < r < 60\mu m$. We notice the existence of a cross-over, occurring at a characteristic length scale ξ , separating small and large scales with two different roughness exponents, i.e. for $r < \xi$, $C(r) \propto r^{\alpha_1}$ and for $r > \xi$, $C(r) \propto r^{\alpha_2}$. The linear fit of $\log(C)$ vs $\log(r)$ in the scaling region, determines the value of the roughness exponent α_1 for small scales and α_2 at large scale. These values are summarized in table II, along with the characteristic length scale ξ .

B. Multifractal properties and singularity spectrum

The global analysis performed above can only reveal the existence of two roughness exponents. In many situations however, rough profiles exhibit a range of roughness exponents. Such profiles are called multifractal while profiles exhibiting a single roughness exponent are called monofractal[27]. Our aim is to determine the full range

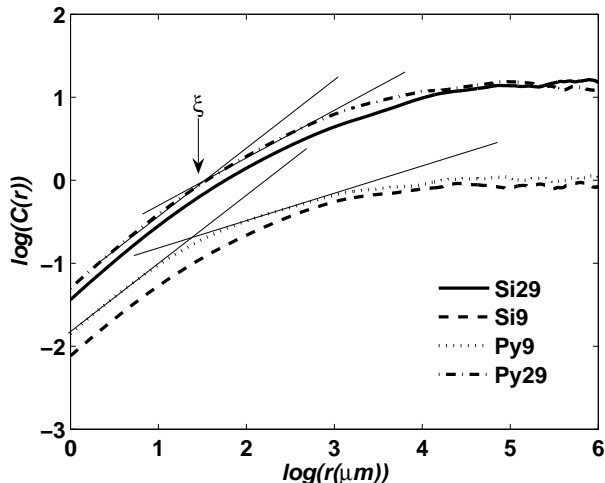


FIG. 2: Plot of the logarithm of the height-height correlation function versus the logarithm of the distance, for Pyrex glass and silicon blasted with alumina particles with sizes of 29 and 9 microns. This plot reveals the existence of a cross-over length scale ξ separating two scaling regions having two different global roughness exponents.

of local roughness exponents for the blasted surfaces using multifractal analysis. To do so, we characterized the profiles by computing the so-called *singularity spectrum*, which determines the distribution of the whole range of local roughness exponents. We used the multifractal detrended fluctuation analysis (MFDFA) [28]. This method has become popular thanks to its simplicity and its easy computer implementation. Other methods exist such as the wavelet transform modulus maxima method (WTMM) [29] but the MFDFA has several advantages [30]. The MFDFA is the extension of the detrended fluctuation (DFA) [31] method which was used to compute the roughness exponent of monofractal signals and for the identification of long range correlations in non-stationary time series [28]. MFDFA is an efficient tool to eliminate undesirable trends in fluctuations. This method applied to our experimental data can be summarized as follow: Given a profile $h(i)$, $i = 1, \dots, N$, we compute the integrated profile,

$$H(i) = \sum_{i=1}^N (h(i) - \langle h \rangle) \quad (3)$$

where N is the number of data points and $\langle h \rangle$ is the mean height of the profile. The whole profile is subdivided into $M_L = N/L$ non-overlapping segments of length L (here L is the number of data points in each segment). Since M_L is not always an integer, some data will be ignored during this procedure. To take them into account, the subdivision is performed from both ends of the profile, which results into $2M_L$ segments. In each segment n the polynomial trend P_n is subtracted from the data. This polynomial is determined by a least square

fit to the data in each segment. Polynomials of degrees higher than 1 can be used, corresponding to MFDFA2, MFDFA3, etc. After detrending in each segment, the variance of the result is calculated :

$$F^2(n, L) = \frac{1}{L} \sum_{j=1}^{j=L} [H((n-1)L+j) - P_n(j)]^2 \quad (4)$$

This expression is then averaged over all segments n and the value of the q^{th} -order fluctuation function is calculated [28]:

$$F_q(L) = \left(\frac{1}{2M_L} \sum_{n=1}^{2M_L} F^2(n, L)^{q/2} \right)^{1/q} \quad (5)$$

Here q is a real number. For a fractal profile $F_q(L)$ follows a power law relation at large scales i.e.:

$$F_q(L) \sim L^{h(q)} \quad (6)$$

The exponent $h(q)$ is called the "generalised Hurst exponent" [28]. For a monofractal profile, $h(q) = \text{const}$ while for a multifractal profile h is a function of q . For positive values of q , $h(q)$ describes the scaling behaviour of the segments with large fluctuations, while for negative values of q , $h(q)$ describes the scaling behaviour of the segments with small fluctuations. The singularity spectrum $f(\alpha)$ is calculated by performing the Legendre Transform [32] of $(q, \tau(q))$ with $\tau(q) = qh(q) - 1$, resulting in:

$$\alpha = \frac{d\tau(q)}{dq} \\ f(\alpha) = q\alpha - \tau(q) \quad (7)$$

The spectrum $f(\alpha)$ can be interpreted as the fractal dimension of a subset of points in the profile characterized by the singularity strength α (the local roughness exponent). For a monofractal profile, $\alpha = \alpha_0$ and $f(\alpha) = 1$, where α_0 is the roughness exponent of the profile. The strength of the multifractality of a profile can be characterized by the difference between the maximum and minimum values of α , i.e. $\Delta\alpha = \alpha_{\text{max}} - \alpha_{\text{min}}$.

Figure 3 shows the logarithm of the fluctuation function ($F_q(d)$) versus the logarithm of the distance $d = L\Delta x$, where Δx is the spatial increment of the profile, for Py29 sample. Also shown is the linear regression fit at large scale for each value of q . We used a detrended polynomial of degree 1 (MFDFA1), but the result remains unchanged when polynomial of degree two and three were used (MFDFA2, MFDFA3). We can see clearly that at large scale, the fluctuation functions $F_q(L)$ are straight lines in the double logarithmic plot, with different slopes indicating the presence of multifractality. In figure 4 the plot of $\tau(q)$ versus q is shown for the four samples Py9, Py29, Si9 and Si29. Note that for $|q| > 5$, the function $\tau(q)$ coincides with its asymptotic form which is a linear function of q [45]. Hence, we choose $-5 \leq q \leq 5$. We notice clearly that $\tau(q)$ is a concave function of function of

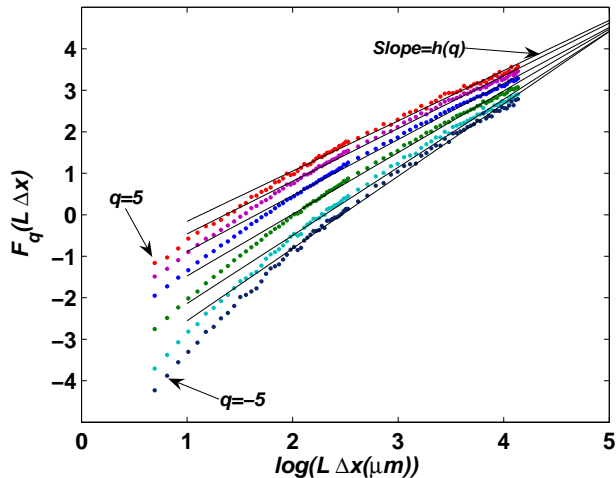


FIG. 3: The logarithm of the fluctuation function $F_q(L\Delta x)$ as a function of the logarithm of the distance $d = L\Delta x$, for Py29 sample, for $q = -5, -3, -1, 1, 3$ and 5 . The straight lines are the regression fits to the data at large scale. The slopes of the lines determine $h(q)$.

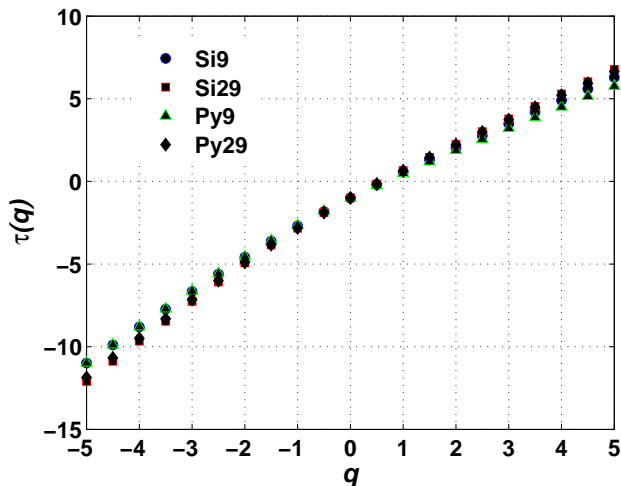


FIG. 4: The q dependence of $\tau(q) = qh(q) - 1$ for the four samples.

q , typical of multifractal profiles. From equations (7) we can estimate the singularity spectrum for the four samples as shown in figure 5. This spectrum is averaged over 12 profile containing 8000 points each. In table III we summarize the values of the strength of the multifractality $\Delta\alpha$ for the four samples.

Sample	Py9	Si9	Py29	Si29
$\Delta\alpha$	0.94	0.8	0.91	0.94

TABLE III: Values of the multifractality strength $\Delta\alpha = \alpha_{min} - \alpha_{max}$ for different samples.

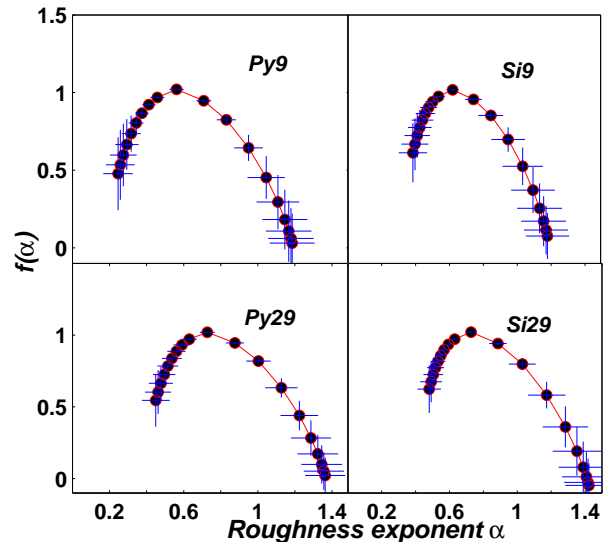


FIG. 5: The singularity spectrum for the four samples. In each case, the spectrum was averaged over 12 profiles containing 8000 points.

IV. DISCUSSION

The values of the two global roughness exponents were determined for all four samples Py9, Py29, Si9 and Si29 using the height-height correlation function. All samples show a crossover behavior corresponding to two values of the roughness exponent α_1 and α_2 shown in table II. The value α_1 is, within the error range, independent of the material or the size of impacting particles. For all analyzed samples, the small scale value is consistent with the approximate universal value of 0.8 found for three dimensional fracture of brittle materials[18, 33, 34]. This provides evidence that at scales below the characteristic length $\xi \sim 5\mu m$, the dominant mechanism in powder blasting is the fracture formation. This observation is in agreement with the static indentation theory[7, 8, 9] where the *dynamic load* of impacting particles creates a local load which increases the local stress resulting in the formation of lateral cracks, which are responsible for the material removal. In general, the universal value of the roughness exponent 0.8 corresponding to three dimensional fracture surfaces is observed at large length scales (from $0.1 \mu m$ to $1 mm$, see reference [16]). In contrast, the dynamic load of impacting particles induces a cross over to smaller values of the global roughness exponent, above $5 \mu m$ (see table II) which are 0.4, 0.32, 0.55 and 0.53 for Si9, Py9, Si29 and Py29, respectively. The large scale values of the global roughness exponent obtained for Py9 and Si9 are smaller than those obtained for Si29 and Py29. The effect of impacting particle's size is felt at large scales. Larger particles give larger roughness exponents, independent of the material being Silicon or Pyrex glass.

We also showed that the surface generated by particles

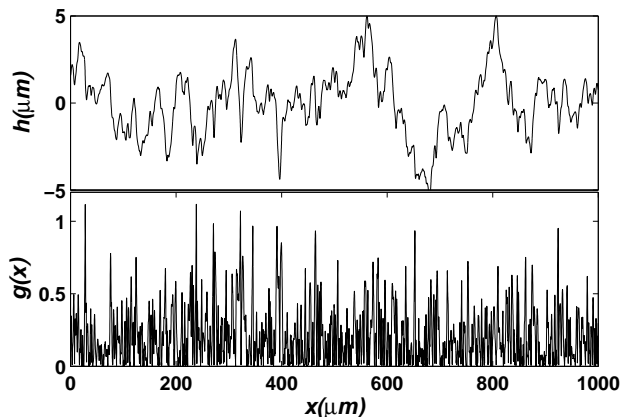


FIG. 6: Top plot, the surface profile of Py29 sample with the corresponding local gradient (bottom plot) showing large fluctuations of the latter which constitutes the signature of intermittency.

blasting share a common property of multifractality. The MF DFA method was used to uncover this property and to determine the singularity spectrum for each four samples. The strengths of multifractality represented by $\Delta\alpha$, as displayed in table III, are close to each other regardless of the size of the particles and the material. This multifractality could be interpreted in terms of spatial intermittency. This concept was argued by Krug [35] to describe the scaling of surfaces generated by epitaxial growth models incorporating very limited atomic mobility leading to a violent spatial intermittent effects and multifractal surfaces. This description was borrowed from fluid turbulence owing the similarity between Galilean invariance of turbulent fluids and translational invariance of interfaces[36]. In our case, we highlight large fluctuations by considering the step size or the gradient at the position $x, g(x) = |\partial h/\partial x|$ for a profile $h(x)$. This quantity is the analog of energy dissipation $\varepsilon = (\partial v/\partial x)^2$, where v is the local velocity of a turbulent fluid[37]. Figure 6 shows the local gradient $g(x)$ for Pyrex glass bombarded by $29\mu m$ -size particles, showing large gradient fluctuations which suggests spatial intermittency. In addition, we consider the distribution of the local gradient in analogy with local velocity gradient in fully developed turbulence, which is described by a stretched exponential distribution[38, 39]. A very similar behaviour is characteristic of all four samples Py9, Py29, Si9 and Si29 as shown in figure 7, where the local gradient distribution fits very well with the stretched exponential function:

$$P(g) = \frac{1}{\Omega} \exp(-ag^\gamma) \quad (8)$$

The fit of the local gradient distribution to equation (8) gives the values of the stretching exponent γ , which are 1.41 ± 0.05 , 1.23 ± 0.03 , 1.37 ± 0.05 and 1.21 ± 0.03 for Si9,

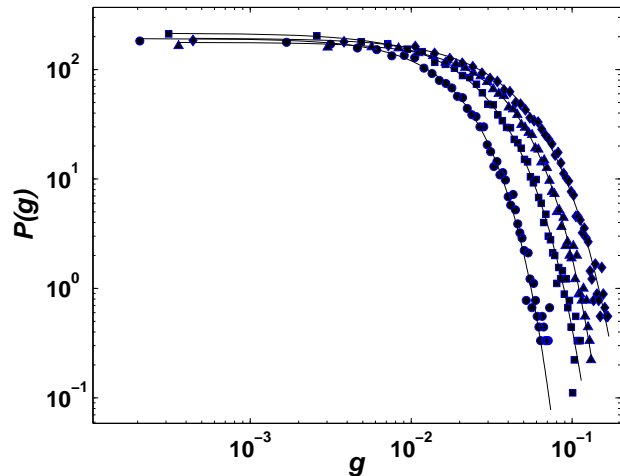


FIG. 7: Local gradient distribution of the four samples Py9(\square), Py29(\diamond), Si9(\circ) and Si29(\triangle). Continuous lines are the fit to the stretched exponential distribution (8).

Py9, Si29 and Py29 respectively. The form of the local gradient distribution suggests that non-linearities must be present at large scale, leading to $h \rightarrow -h$ symmetry breaking. Indeed, the skewness s of the profiles for all samples are non-zero and have the values $s \simeq -0.4, -0.35, -0.28$ and -0.4 for Si9, Si29, Py9 and Py29 respectively. We can now ask the question: What is the origin of the observed multifractality? It well known that multiplicative cascades [37, 40] models generate processes known to have intermittent behaviour and a multifractal character, mirroring the presence of intermittent fluctuations with long-range correlations. These long-range correlations are generated at large scale by features that hierarchically cascade their influence to smaller scales. To detect the presence of long range correlations in our surface profiles, we perform the following test[41]: we generated a surrogate data set by shuffling the height data in each profile. The newly generated data set preserves the distribution of the height but destroys the long range correlations, which means that the surrogate profiles will exhibit a monofractal behavior, if the multifractality originates from the long-range correlations and not from the height distribution. We performed the MF DFA and found that the surrogate data set is monofractal with the roughness exponent $\alpha = 0.5$ for all for samples. Thus, the observed multifractal behaviour is a result of long range correlations since the shuffling procedure preserves the height distribution. The effect of long-range elastic interaction in developing long-range correlations was reported by some authors in the case of elastic chains driven in a quenched random pinning [42], or during crack propagation [43]. Undoubtedly a detailed theoretical investigation is needed in order to determine the origin of the long-range correlations in sharp particle's bombardment of brittle materials.

V. CONCLUSION

In conclusion we conducted a detailed scaling analysis of surfaces of two brittle materials, Silicon and Pyrex glass, after bombardment with alumina particles of two different sizes $9\mu\text{m}$ and $29\mu\text{m}$. The bombardment results in multifractal surfaces. This multifractality is common to all samples regardless of the nature of the material or the size of the particles. We determined the corresponding singularity spectrum revealing a broad range of

scaling exponents. We argued that for scales below $5\mu\text{m}$, fracture processes are dominant while at large scales long range correlations are responsible for the observed multifractal behavior.

Acknowledgments

The authors would like to thank E. Bouchaud for the useful discussions.

-
- [1] P. Slikkerveer, P. Bouten, and F. de Haas, *Sensors and Actuators* **85**, 296 (2000).
 - [2] S. Belloy, E. Thurre, A. Walckiers, Sayah, and M. Gijs, *Eurosensors XIII proceeding, the Hague, Holland* p. 827 (1999).
 - [3] T. T. Veenstra, J. W. Berenschot, J. G. E. Gardeniers, R. G. P. Sanders, M. C. Elwenspoek, and A. van den Berg, *J. Electrochem. Soc.* **148**, G68 (2001).
 - [4] S. Schlautmann, H. Wensink, R. M. Schasfoort, M. Elwenspoek, and A. V. D. Berg, *J. Micromech. Microeng.* **11**, 386 (2001).
 - [5] P. J. Slikkerveer, P. Bouten, F. in't Veld, and H. Scholen, *Wear* **217**, 237 (1998).
 - [6] X. Chen, J. W. Hutchinson, and A. G. Evans, *J. Am. Ceram. Soc.* **88**, 1233 (2005).
 - [7] B. R. Lawn and E. R. Fuller, *J. Mater. Sci.* **10**, 2016 (1975).
 - [8] D. B. Marshall, B. R. Lawn, and A. G. Evans, *J. Am. Ceram. Soc.* **65**, 561 (1982).
 - [9] R. F. Cook and G. M. Pharr, *J. Am. Ceram. Soc.* **73**, 787 (1990).
 - [10] A. G. Evans and T. R. Wilshaw, *Acta Mater.* **24**, 939 (1976).
 - [11] B. R. Lawn, *J. Am. Ceram. Soc.* **81**, 1977 (1998).
 - [12] A. G. Evans and E. A. Charles, *J. Am. Ceram. Soc.* **59**, 371 (1976).
 - [13] J. T. Hagan and M. V. Swain, *J. Phys. D: Appl. Phys.* **11**, 2091 (1978).
 - [14] I. Finnie, *Wear* **186**, 1 (1995).
 - [15] B. Lawn, *Fracture of Brittle Solids 2nd edn* (Cambridge University Press, 1993).
 - [16] E. Bouchaud, *J. Phys.: Condens. Matter* **9**, 4319 (1997).
 - [17] F. Family and T. Viscek, *Dynamics of Fractal Surfaces* (World Scientific, Singapore, 1991).
 - [18] K. J. Måløy, A. Hansen, E. L. Hinrichsen, and S. Roux, *Phys. Rev. Lett.* **68**, 213 (1992).
 - [19] J. Schmittbuhl, S. Roux, and Y. Berthaud, *Europhys. Lett.* **28**, 585 (1994).
 - [20] V. Y. Milman, R. Blumenfeld, N. A. Stelmashenko, and R. C. Ball, *Phys. Rev. Lett.* **71**, 204 (1993).
 - [21] V. Y. Milman, N. A. Stelmashenko, and R. Blumenfeld, *Prog. Mater. Sci.* **38**, 425 (1994).
 - [22] P. McAnulty, L. V. Meisel, and P. J. Cote, *Phys. Rev. A* **46**, 3523 (1992).
 - [23] J. P. Bouchaud, E. Bouchaud, G. Lapasset, and J. Plans, *Phys. Rev. Lett.* **71**, 2240 (1993).
 - [24] D. Ertas and M. Kardar, *Phys. Rev. Lett.* **66**, 929 (1992).
 - [25] D. Ertas and M. Kardar, *Phys. Rev. E* **48**, 1703 (1993).
 - [26] A. Nakano, R. K. Kalia, and P. Vashishta, *Phys. Rev. Lett.* **75**, 3138 (1995).
 - [27] L. Calvet, A. Fisher, and B. B. Mandelbrot, *Cowles Foundation paper 1164* (unpublished).
 - [28] J. W. Kantelhardt, S. A. Zschiegner, E. Koscielny-Bunde, S. Havlin, A. Bunde, and H. E. Stanley, *Physica A* **316**, 87 (2002).
 - [29] J. F. Muzy, E. Bacry, and A. Arneodo, *Phys. Rev. Lett.* **67**, 3515 (1991).
 - [30] P. Oświęcimka, J. Kwapien, and S. Drożdż, *Phys. Rev. A* **46**, 3523 (1992).
 - [31] C. K. Peng, S. V. Buldyrev, S. Havlin, M. Simons, H. E. Stanley, and A. L. Goldberger, *Phys. Rev. E* **49**, 1685 (1994).
 - [32] J. Feder, *Fractals* (Plenum Press, New York, 1988).
 - [33] E. Bouchaud, G. Lapasset, and J. Planés, *Europhys. Lett.* **13**, 73 (1990).
 - [34] J. Schmittbuhl, F. Schmitt, and C. Scholz, *J. Geophys. Res.* **100**, 5953 (1995).
 - [35] J. Krug, *Phys. Rev. Lett.* **72**, 2907 (1994).
 - [36] T. Bohr, G. Grinstein, C. Jayaprakash, M. H. Jensen, J. Krug, and D. Mukamel, *Physica A* **59D**, 177 (1992).
 - [37] U. Frisch, *Turbulence: the legacy of A. N. Kolmogorov* (Cambridge University Press, 1995).
 - [38] A. Bershadskii, *Europhys. Lett.* **39**, 587 (1997).
 - [39] P. Kailasnath, K. R. Sreenivasan, and G. Stolovitzky, *Phys. Rev. Lett.* **68**, 2766 (1992).
 - [40] B. Mandelbrot, *On Intermittent Free Turbulence, Turbulence of Fluids and Plasmas* (Interscience, New York, 1969).
 - [41] P. C. Ivanov, L. A. N. Amaral, A. L. Goldberger, S. Havlin, Michael, G. Rosenblum, Z. R. Struzick, and H. E. Stanley, *Nature* **399**, 461 (1999).
 - [42] A. Tanguy, M. Gounelle, and S. Roux, *Phys. Rev. E* **58**, 1577 (1998).
 - [43] H. Gao and J. R. Rice, *J. Appl. Mech.* **56**, 828 (1989).
 - [44] L. Calvet, A. Fisher, and B. B. Mandelbrot (1997), *Cowles Foundation Discussion Paper No. 1165*.
 - [45] Note that the function $\tau(q)$ defined in the MF DFA formalism, is equivalent to functions defined in standard multifractal formalism. For rigorous definitions and properties of $\tau(q)$ see for example [44].